


Article

Ultrashort Vortex Pulses with Controlled Spectral Gouy Rotation

Max Liebmann ^{1,2}, Alexander Treffer ¹, Martin Bock ¹, Ulrike Wallrabe ³ and Ruediger Grunwald ^{1,*} 

¹ Max Born Institute for Nonlinear Optics and Short-Pulse Spectroscopy, 12489 Berlin, Germany; max.liebmann@holoeye.com (M.L.); Alexander.Treffer@mbi-berlin.de (A.T.); mbock@mbi-berlin.de (M.B.)

² HOLOEYE Photonics AG, 12489 Berlin, Germany

³ IMTEK-Department of Microsystems Engineering, University of Freiburg, 79110 Freiburg im Breisgau, Germany; wallrabe@imtek.uni-freiburg.de

* Correspondence: grunwald@mbi-berlin.de

Received: 29 May 2020; Accepted: 18 June 2020; Published: 22 June 2020



Featured Application: Controlling the spectral Gouy rotation of propagating pulsed beams with orbital angular momentum opens specific channels for ultrafast communication and excitation.

Abstract: Recently, the spatio-spectral propagation dynamic of ultrashort-pulsed vortex beams was demonstrated by 2D mapping of spectral moments. The rotation of characteristic anomalies, so-called “spectral eyes”, was explained by wavelength-dependent Gouy phase shift. Controlling of this spectral rotation is essential for specific applications, e.g., communication and processing. Here, we report on advanced concepts for spectral rotational control and related first-principle experiments. The speed of rotation of spectral eyes during propagation is shown to be essentially determined by angular and spectral parameters. The performance of fixed diffractive optical elements (DOE) and programmable liquid-crystal-on silicon spatial light modulators (LCoS-SLMs) that act as spiral phase gratings (SPG) or spiral phase plates (SPP) is compared. The approach is extended to radially chirped SPGs inducing axially variable angular velocity. The generation of time-dependent orbital angular momentum (self-torque) by superimposing multiple vortex pulses is proposed.

Keywords: orbital angular momentum; vortex beams; femtosecond pulses; structured beams; spiral gratings; Gouy phase shift; spectral Gouy rotation; spectral anomalies

1. Introduction

Orbital angular momentum (OAM) beams or vortex beams [1–4] propagate with twisted wavefronts and belong to “core concepts” in optical technologies [5]. Their topological charges are a measure of OAM density. The specific topological degrees of freedom can be exploited for optical tweezing [6–8], momentum transfer to atoms and molecules [9,10] microstructuring of materials [11–14], microscopy [15], optical processing [16], communication [17–20], and other advanced applications [21,22]. For information transfer, tuning and switching of topological charges is an obvious option. In addition to the azimuthal degrees of freedom, the axial propagation characteristics can be structured as well. It was found that an axial shaping of local topological charges can be obtained by the interference of multiple Bessel-like modes, while the OAM is globally conserved [23]. The influence of amplitude and phase gradients as well as intensity-induced nonlinearities on the vortex propagation was investigated [24,25].

The combination of twisted wavefront and ultrashort pulse duration opens specific channels for high-data-rate optical communication, nonlinear excitation, or optical processing. Ultrafast singular

optics is per se polychromatic and enables for multidimensional structuring of light in spectral, temporal, and spatial domains. At extremely short pulse durations, spatio-temporal coupling effects caused by pulse travel-time and angular geometry can lead to highly complex propagation effects and related limitations of the topological charge spectrum [26]. At moderate pulse durations and corresponding spectral bandwidths in 10-nm range, however, space-time coupling can typically be neglected. Instead, spatio-spectral maps in the vicinity of phase singularities reveal kinds of spectral anomalies with peculiar properties, so-called “spectral eyes”. Spectral eyes have been well-known in singular optics for a relatively long time [27–34] and represent regions with blue- and red-shifted spectral centers of gravity (COG) of polychromatic OAM light fields. The spectral redistribution basically results from wavelength-dependent diffraction at a phase discontinuity, e.g., the phase step of a spiral phase plate (SPP), the transition between regions of different spatial frequencies in a forked grating or the asymmetric phase structure of a spiral phase grating (SPG). In all cases, the vortex is generated by symmetry-breaking geometrical configurations.

Recently, we found that, for appropriately chosen parameters, spectral eyes of Bessel–Gauss beams with OAM undergo a characteristic rotation during pulse propagation [35]. This behavior was explained by a wavelength-dependent Gouy phase shift of a polychromatic vortex and therefore referred to as “spectral Gouy rotation” [36,37]. Until that point, the influence of the Gouy phase on the propagation dynamics was mostly discussed with respect to rotating intensity patterns [38]. From experiments with distorted OAM beams, it was also known that an initial intensity distortion leads to rotation in intensity maps as a function of the axial distance of the detection plane [39]. This type of rotation directly reflects the wavefront twist and can be applied to metrology applications. For precise translation measurements, e.g., revolutions of multi-zeros can be counted [40], and interferometry with conjugate twisted beams is another option [41]. Unlike OAM vortices, vector vortices are based on the spin angular momentum and can be tuned by polarization control. With pairs of chirped vortex pulses and polarization-dependent vortex conversion, ultrafast rotating ring-shaped intensity lattices were obtained and applied to the coherent excitation enhancement of a quasi-particle [42]. Variable intra-pulse rotation (“self-torque”) was obtained by superposition of chirped vortex pulses [43].

In contrast to the rotating intensity patterns, spectral Gouy rotation is a more subtle effect. On the one hand, related experiments appear to be more complicated. On the other hand, the access to specific, usually hidden degrees of freedom enables alternative concepts of encryption, computing, or measuring techniques. An essential precondition for potential applications is to identify the key parameters for adjusting spectral Gouy rotation. Here, we report on the results of proof-of-principle experiments with the aim to control the angular frequency of the rotating spectral eyes. The performance of different types of spiral phase shapers is compared [44]. The generation of axially variable angular velocity by a programmable, radially chirped spiral grating is demonstrated. Moreover, in analogy to the most recently introduced concept of “self-torque” [43], a method for intrapulse rotational management in spectral domain via rotational beating of multiple OAM beams is proposed.

2. Theoretical Background and Numerical Simulation

2.1. Spectral Gouy Rotation of Bessel–Gauss Beams

Spectral rotation properties of OAM pulses result from the coaction of wavefront rotation and Gouy effect. The wavefront rotation in polychromatic singular beams is determined by the spectral distribution function, either because of the wavelength-dependence of the diffraction angle (for spiral gratings) or because of the spectral dependent mismatch of the phase shift of polychromatic beams (for spiral phase plates). The Gouy phase shift [45–47] is a characteristic phase delay of a beam at passing a focal region which amounts to π for Gaussian beams. The phenomenon can be explained by a geometrical path length difference [48] or as a consequence of the uncertainty relation in transversal confinement [49]. To obtain a continuing rotation of spectral eyes around the phase singularities, two necessary preconditions have to be fulfilled. At first, the spectral bandwidth should enable

for a measurable separation of blue- and red-shifted parts. At near-infrared wavelengths, spectral eyes were shown to be reliably detectable at bandwidths in the range of 10 nm [37]. Secondly, the wavelength-dependent Gouy rotation has to be accumulated with increasing propagation distance. This condition is matched if the focus is replaced by continuously superimposing conical partial beams, as it is the case for nondiffracting Bessel or Bessel–Gauss beams [49]. By solving the transverse Helmholtz equation, it can be shown that the wavelength-dependent extra phase shift $\Delta\psi_B$ of a Bessel beam compared to a reference plane wave accumulates with the distance z [50]:

$$\Delta\psi_B(\lambda) = (k - \beta)z \quad (1)$$

Here, k and β are the amount of the wave vector and the propagation constant, respectively. In contrast to Hermite–Gaussian and Laguerre–Gaussian beams, the Gouy phase shift is independent on the order of the Bessel beam. The spatial confinement of the Bessel beam can be described by a parameter.

$$\alpha = \sqrt{k^2 - \beta^2} \quad (2)$$

so that, with Equations (1) and (2), the propagation dependent spectral Gouy phase shift can also be written in terms of the confinement factor

$$\Delta\psi_B(\lambda) = \frac{\alpha^2}{k + \sqrt{k^2 - \alpha^2}}z \quad (3)$$

For ultrashort pulses with extremely broad spectra and high intensity, specific spatio-temporal chirp phenomena should modify the Gouy phase shift because of dispersion and nonlinear optical distortions. Under the conditions our experiments, i.e., working with Bessel–Gauss-type vortex beams of low pulse energies and few-nm spectral widths, such additional effects were mostly negligible.

2.2. Numerical Simulation

For the numerical analysis of the beam dynamics, 2D-maps of local spectral intensity distributions $S(x,y,\lambda)$ were calculated for propagation distances z . Simulations were performed on the basis of a simplified model with the wave-propagation software VirtualLab 7.5 (LightTrans, Jena, Germany). In particular, Gaussian spectral distributions with a full-width-at-half-maximum (FWHM) bandwidth of 12 nm were assumed, which approximates realistic experimental conditions. A binary spiral phase grating with a period of 8 μm and a phase stroke of 2π (related to a wavelength of 800 nm) was illuminated by a Gaussian beam with a waist radius of $w_0 = 100 \mu\text{m}$ to emulate the diffraction at components with small apertures. To filter out essential features of the obtained spatio-spectral maps, local statistical moments $M^{(i)}(x,y,\lambda)$ were determined. At the same time, this kind of spectral image processing procedure also enables one to reduce the large data containing fully extended spectra for each point in space. Figure 1 shows the results of the numerical simulations in terms of centers of gravity (COG), i.e., first spectral moments $M^{(1)}(x,y)$ for selected values of z between 4 and 11 mm increasing in steps of $\Delta z = 0.5 \text{ mm}$ (see also the visualization movie in the supplementary material). The color code of the graphics reaches from about 793 nm (blue-shifted parts) until about 808 nm (red-shifted parts). The limits of the spectral interval slightly change depending on the axial distance to best visualize the spectral maps. The variation of the applied scale, however, did not exceed a value of 0.9 nm. The divergent Gaussian beam causes a stretching of the spatial scale with increasing distance.

This rough numerical simulation enables one to draw up some predictions about the spatio-spectral propagation characteristics. The doublets of blue-and red-shifted extremal areas (spectral eyes) are expected to rotate around the phase singularity, (2) the spatial extension of spectral eyes is not constant, and spectral bandwidth and center of gravity appear to be slightly varying. Thus, the simulation of propagating spectral maps describes an angular rotation together with specific, oscillating spatio-spectral distortions, which were studied more in detail in our experiments.

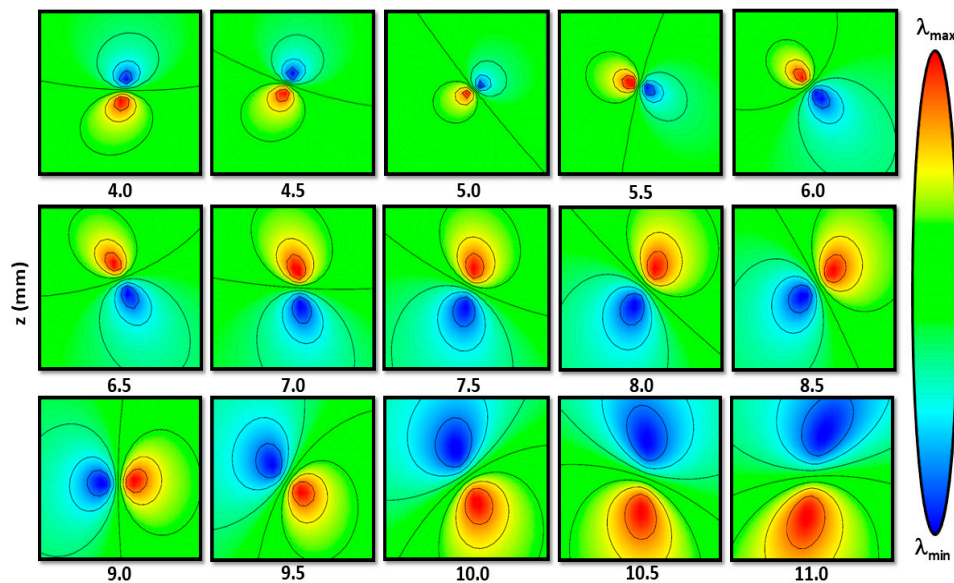


Figure 1. Numerical simulation of rotating anomalies in the spatio-spectral propagation of femtosecond vortex pulses in air ($\text{FOV} = 12 \times 12 \mu\text{m}^2$). The centers of gravity (COG) of local spectral moments at distances z between 4 and 11 mm show the circulation of spectral eyes around the singularity during a full period of spectral Gouy rotation. To induce the orbital angular momentum, a binary spiral phase grating with a period of $8 \mu\text{m}$ and a phase stroke of 2π at a central wavelength of 800 nm was illuminated by a Gaussian beam of a full-width-at-half-maximum (FWHM) spectral bandwidth of 12 nm with a waist radius of $w_0 = 100 \mu\text{m}$. The color code reaches from a lower limit (blue tail) of $\lambda_{\min} = 793 \text{ nm}$ to an upper limit (red tail) of $\lambda_{\max} = 808 \text{ nm}$ ($\pm 0.9 \text{ nm}$).

3. Experimental Techniques and Mathematical Tools

3.1. Shaping of Femtosecond Vortex Pulses with Stationary and Adaptive Components

The experimental setup for rotational pulse control in spectral domain with pulsed polychromatic Bessel–Gauss beams is schematically drawn in Figure 2. The studies were performed with a linearly polarized Ti: sapphire laser oscillator as the light source (Tsunami, Spectra Physics, formerly Mountain View, CA, USA) maximum spectral FWHM width 12 nm , minimum pulse duration 80 fs , central wavelength 795 nm , repetition rate 80.2 MHz , pulse energy $< 8 \text{ nJ}$ [44]. The capability of adaptive and passive optical components to generate OAM beams with variable spatio-spectral parameters, in particular to control the spectral Gouy rotation of pairs of blue-and red-shifted spectral eyes, was studied. Bessel–Gauss beams were either shaped by static lithographically structured, transmissive spiral phase gratings (SPG) [51–53] and continuous-relief spiral phase plates (SPPs) [54], or spiral and forked gratings flexibly programmed into the phase map of a liquid-crystal-on-silicon (LCoS) spatial light modulator (SLM) (GAEA 2, HOLOEYE Photonics AG, Berlin, Germany) [44]. The SLM enables one to individually address 4160×2464 pixels with $3.74 \mu\text{m}$ pitch at a fill factor of 90% with a frame rate of 58 Hz and 8 Bit dynamic range. The reflective operation mode requires working at an oblique angle of incidence to avoid the insertion of dispersive beam splitters. The resulting geometrical distortions in one spatial direction can easily be corrected by an adapted linear transformation (stretching or shrinking) with the programmable display [44]. The average laser power density on the SLM was always chosen to ensure a linear operation.

With the scanning fiber-coupled spectrometer, full local spectra were detected for each distance z and further processed with advanced statistical methods [55].

Areas in the proximity of the phase singularities with diameters at few-micrometer scale were sampled with a truncated fiber (detecting aperture $10 \mu\text{m}$) in combination with a $100\times$ achromatic microscope (Carl Zeiss). To reconstruct the spectral propagation characteristics, two-dimensional

maps of complete local spectra for variable axial distances z were analyzed in a first step by a grating spectrometer (AvaSpec-2048-USB2, Avantes, 600 lines/mm grating, <0.7 nm resolution, 2048 pixel CCD ILX554, Sony, Avantes, Apeldoorn, The Netherlands). In a second step, the spectra were post-processed. The positioning accuracy of the three-axis translation stages (AG-LS 25–27, Newport) was limited to ± 100 nm. The spectral resolution was found to be closely sufficient to clearly indicate the relevant spectral structures. In addition to sequential spectral scanning, intensity patterns were monitored by a high-quantum-efficiency EMCCD camera (iXon, Andor Technology, Belfast, UK).

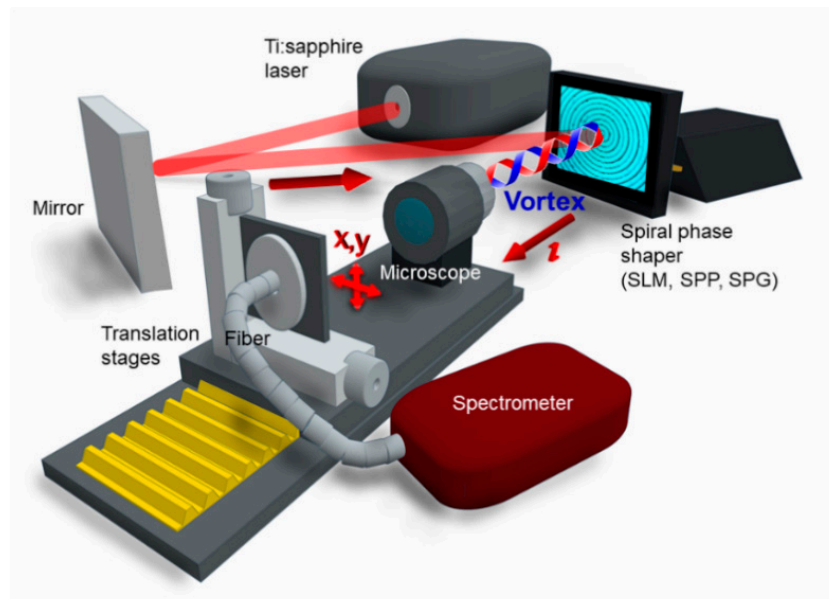


Figure 2. Experimental setup for the generation and detection of femtosecond vortex pulses. An orbital angular momentum is induced by optional use of a spatial light modulator (SLM), a transmissive diffractive spiral phase grating (SPG), or a reflective spiral phase plate (SPP) as beam shaper. The vortex is magnified by a microscope and analyzed in spectral domain by a scanning fiber-based spectrometer. The fiber is moved by high-precision xyz-translation stages. From detected local spectra, 2D maps of spectral statistical moments $M^{(j)}(x,y)$ are extracted for each distance z .

3.2. Vortex Analysis with Spectral Statistical Moments

Alongside the general possibility to optimize spatio-temporal pulse transfer, the specific potential of controlling the rotational properties of spectral anomalies to optical information encoding is a further rewarding goal of spectral vortex manipulation. Previously, it was proposed to exploit spectral shifts and spectral switches caused by phase singularities [34,56], which are also observed in polychromatic double slit interference patterns [57]. A central problem for the necessary information processing in all of these cases is the development of appropriate mathematical tools for filtering out and quantitatively describing particular spectral patterns, flow structures, and rotational transformations. Therefore, tailored statistical approaches were applied in our experimental investigations.

To reduce the amount of data and to extract essential features of vorticity, local spectral moments $M^{(j)}(x,y)$ and linear combinations of such were determined for each transversal coordinate (x,y) in a plane. The resulting “movies” of z -dependent moment maps $M^{(j)}(x,y,z)$ specifically describe the spectral propagation behavior. The index j indicates the order of the statistical moment. The moments for $j = 1$ to $j = 4$ are related to center of gravity (COG), standard deviation, skewness, and kurtosis. More details on the statistical methods, including an extension to global moment analysis with radial meta-moments, were reported in ref. [55].

3.3. Rotation Control and Relevant Parameters

To control the spectral Gouy rotation, key influencing parameters have to be identified. The dependence of the Gouy phase shift on the wavelength and the conical beam angle enables one to adjust the spectral rotation by (a) shaping the spectral distribution function and (b) shaping the angular profile. The spectral parameters can be influenced by tuning the center wavelength of the source by mode management, or spectral filtering. The angular profile can be adjusted by grating periods of spiral shapers and by the divergence or convergence of the illuminating beam. For microoptical vortex generators, the diffraction at the edges essentially contributes to the angular profile so that the Fresnel number of the aperture also has to be taken into account as an additional relevant parameter.

Furthermore, radial gradients of spectral and/or angular parameters can be exploited to axially tune the rotation velocity. In time domain, a slow tuning by spatial light modulation with piezo-actuated or liquid-crystal spiral phase shapers or a fast tuning by intrapulse frequency chirp is possible. The experiments to be presented here were focused on the variation of bandwidth, center wavelength, grating period, and aperture diameter.

The identification of COG positions of spectral eyes as a function of the propagation distance z provides a simple description of the helical spectral characteristics of interest. From the axial rotation cycles, which will be referred to as “periods”, an axial angular velocity Ω_z can be defined as the axial derivative of the rotation angle φ of the connecting line between these COG coordinates:

$$\Omega_z = \frac{d\varphi}{dz} \quad (4)$$

The related temporal angular velocity Ω_t follows as

$$\Omega_t = \frac{d\varphi}{dt} = c \cdot \Omega_z \quad (5)$$

where $c = z/t$ is the velocity of light in vacuum. For a constant axial angular velocity (comparable to the “thread pitch” of a screw), the number of axial and temporal periods P_0 and $T_0 = P_0/c$ within a given propagation distance z is directly proportional to Ω_z and Ω_t , respectively. The rotation angle as a function of the distance can be written as

$$\varphi(z) = 2\pi \frac{z}{P_0} \quad (6)$$

In general, however, the axial angular velocity can be a function of propagation distance z and propagation time t , and variable axial and temporal periods $P(z)$ and $T(t) = P(z)/c$ can be determined. In this case, equation (6) cannot be applied and has to be replaced by a differential approach:

$$\frac{d\varphi(z)}{dz} = \frac{2\pi}{P(z)} \quad (7)$$

Because of the relationship between spatial and temporal rotation, the distance-dependent spectral Gouy rotation of light pulses in flight can be interpreted as an ultrafast temporal phenomenon correlated to dynamic spectral maps. In both cases, the actual information can be encoded in first- or higher-order derivatives of the rotation angle of the spectral anomalies. For example, radial periodicity gradients of spiral gratings can be used to modulate the axial angular velocity. To further extend the range of free parameters, rotation velocity and rotational acceleration can also be combined with targeted modifications of the statistical moments of the spectral eyes.

4. Experimental Results and Discussion

4.1. Parameters of Applied Spiral Phase Shapers

Relevant geometrical parameters for Spiral Phase Gratings (SPGs) as used in our experiments are listed in Table 1 [44]. To quantitatively compare the influence of diffraction, Fresnel numbers for half of the axial focal zone depths at a central wavelength of 800 nm are included. Microscope images of central parts of three selected spiral gratings of Table 1 are shown in Figure 3.

Table 1. Geometrical parameters of spiral phase gratings used as orbital angular momentum (OAM) beam shapers.

Spiral Phase Gratings (SPG) Con-Figuration	Type of Orbital Angular Momentum (OAM) Shaper	Grating Period (μm)	Aperture Diameter (mm)	Depth of Focal Zone (mm)	Fresnel Number (Aperture) ¹	1st Order Diffraction Angle ($^\circ$)
1	SLM_32	32	2	40	250	1.43
2	SLM_16	16	2	20	500	2.87
3	DOE 4-step	16	2	20	500	2.87
4	DOE 2-step	16	0.4	4	100	2.87
5	DOE 2-step	16	0.2	2	50	2.87
6	DOE 2-step	32	0.4	8	50	1.43

¹ Data related to half depth of each focal zone at a central wavelength of 800 nm.

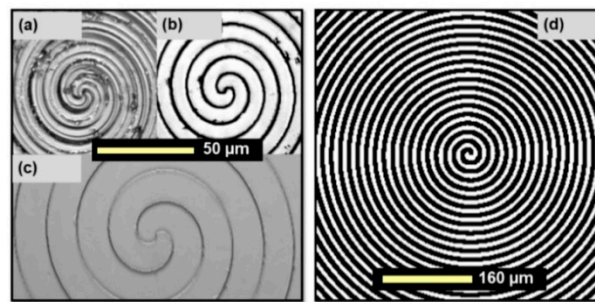


Figure 3. Parts of selected spiral phase gratings (SPGs) used as vortex beam shapers in the experimental studies: (a–c) fixed diffractive elements (left) and (d) spiral structure programmed into the SLM grey scale map (right). The elements correspond to configurations 3, 4, 6, and 2 in Table 1, respectively.

4.2. Spectral Control by Tuning Center Wavelength and Bandwidth

To study the influence of a variation of spectral input parameters on the spectral moments, slight modifications of center wavelengths and FWHM bandwidth were induced (Figure 4a,b). Three closely neighboring central wavelengths were generated.

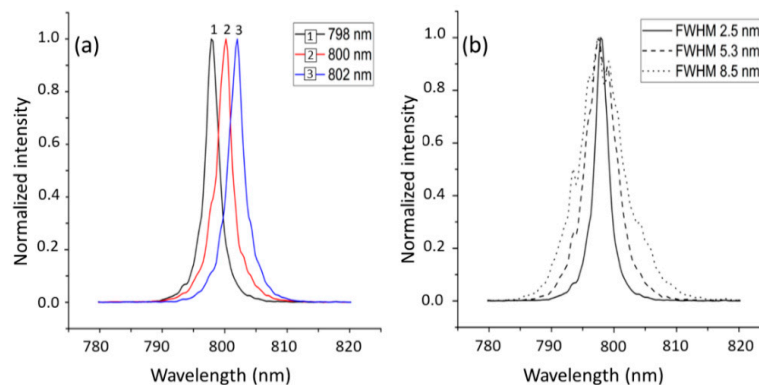


Figure 4. Spectral control by (a) tuning the center wavelength via laser mode adjustment (1–3: three states shown with center wavelengths at 798 nm, 800 nm, and 802 nm, respectively), (b) varying the FWHM spectral bandwidth $\Delta\lambda$ for a single selected laser mode (center wavelength $\lambda_0 = 798$ nm) between 2.5 nm and 8.5 nm.

As expected, an increasing input spectral bandwidth results in an extended bandwidth in the spectral eyes as demonstrated in Figure 5. The transfer characteristics also enable one to identify the ranges for channel separation without spectral overlap, which may be relevant for practical applications. To avoid misinterpretations, it has to be addressed that the essential information in the curves is not a bandwidth transfer. The pairs of curves are related to the spectral eyes, each upper curve of a pair corresponds to the red-shifted part, and each lower curve to the blue-shifted one, respectively. The ordinate values represent the spectral coordinates of the spectral eyes. Their distance is not directly a measure of the output bandwidth.

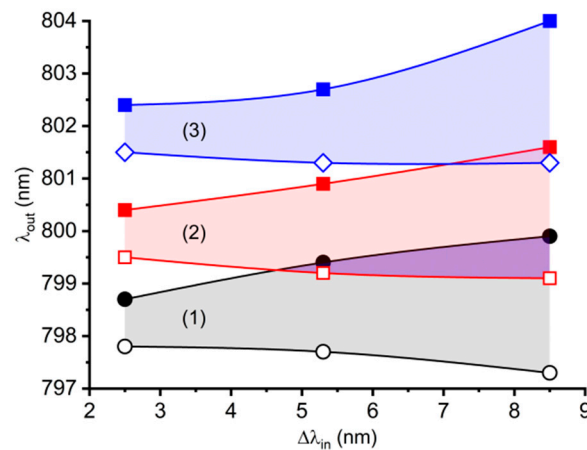


Figure 5. Spectral transfer into vortex beams as a function of input spectral FWHM bandwidth for three wavelength ranges around (1) 798 nm, (2) 800 nm, and (3) 802 nm (spectral profiles in Figure 4a). Filled symbols: upper limits, hollow symbols: lower limits of spectral content in the spectral eyes.

4.3. Variation of Grating Parameters

A variation of the axial angular velocity Ω_z of the spectral Gouy rotation was obtained by (i) subsequently inserting static SPGs with different structural periods, and (ii) by adaptively modifying the periods of spiral phase gratings programmed into grey value maps of an LCoS-SLM.

The diameter of the illuminating beam was about 4 mm, and the generated OAM beams were regarded to be Bessel–Gauss beams. For the smallest elements, this diameter was by a factor of 20 larger compared to the element diameter, so a plane wave illumination was assumed. The set of propagation-dependent first spectral moment (COG) maps in Figure 6a clearly indicates the spectral Gouy rotation for a particular configuration. Here, the SPG acts as an axicon and generates a Bessel–Gauss beam with OAM accumulating the spectral Gouy phase shift. In the second configuration in Figure 6b, the phase is only shifted axially by a staircase-like phase profile of a programmed SPP. In this case, no significant spectral Gouy rotation appears because the phase shift is not accumulated (there is no Bessel-like beam).

It should be mentioned that a simple control of the rotation is even possible in the second case if the SPP phase map on the SLM is rotated. This trivial approach enables one to easily change the direction of rotation and to realize arbitrary angles at each distance.

By varying the geometrical parameters, the angular velocity of spectral Gouy rotation can be controlled over an extended range. This is demonstrated in Figure 7 for programmable (SLM) and fixed (DOE) configurations by comparing the rotation cycles for equal propagation paths Δz . Grating structure periods p and overall diameters D are found in the Figure caption.

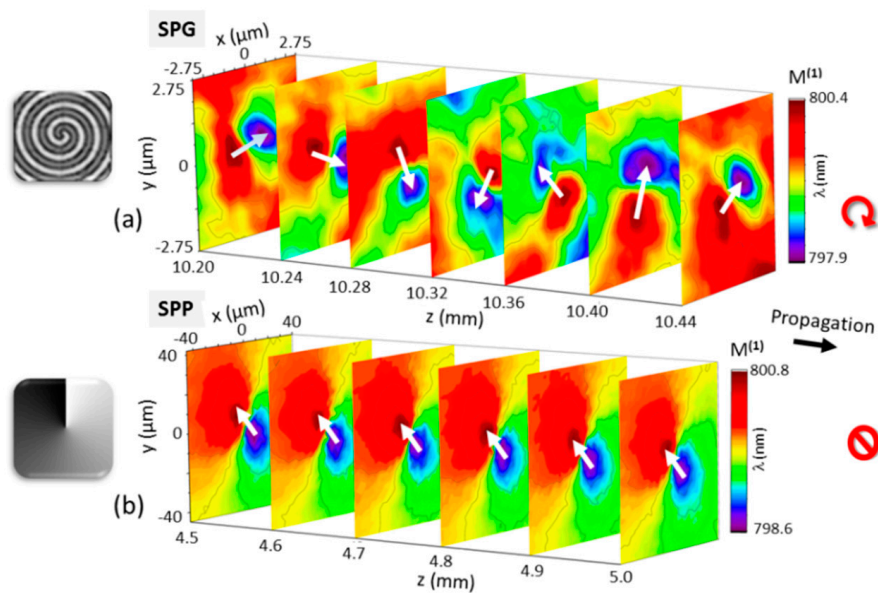


Figure 6. Propagation-dependent maps of 1st spectral moment (COG) of experimentally detected maps of local spectra for two different vortex shaper configurations programmed in an LCoS-SLM (aperture $D = 2$ mm): (a) generation of a Bessel–Gauss beam with a spiral phase grating (SPG) with spectral Gouy rotation (spiral grating period $p = 16$ μm) (see also video S1 in the supplementary material); (b) vortex generation with a spiral phase plate (SPP), without spectral Gouy rotation. The little grey scale pictures at the left side symbolize the type of element (SPG, SPP).

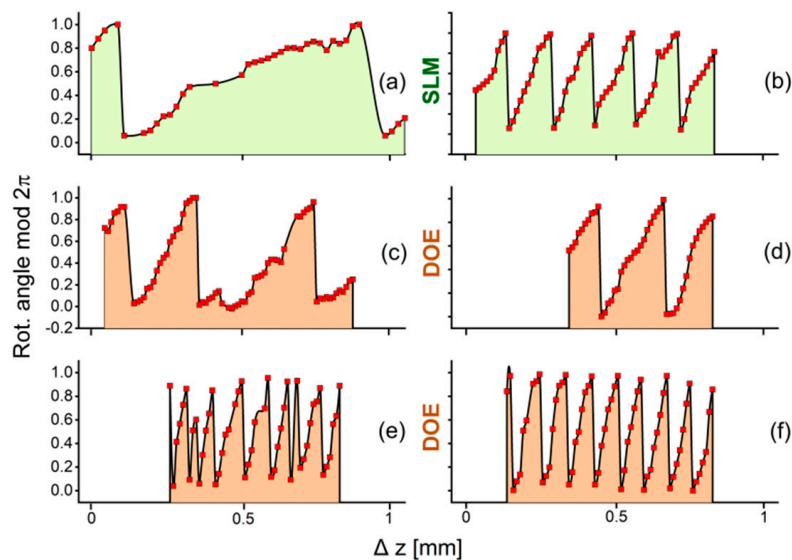


Figure 7. Controlling the angular velocity by varying geometrical parameters. The modulo of the rotation angle is plotted as a function of propagation distance for equal paths Δz . Different grating structure periods p and overall diameters D for programmable (SLM) and fixed (DOE) configurations are compared: (a) SLM, $p = 32$ μm , $D = 2$ mm; (b) SLM, $p = 16$ μm , $D = 2$ mm; (c) DOE, $p = 32$ μm , $D = 0.4$ mm; (d) DOE, $p = 16$ μm , $D = 2$ mm; (e) DOE, $p = 16$ μm , $D = 0.2$ mm; and (f) DOE, $p = 16$ μm , $D = 0.4$ mm.

The related parameter space is presented in Figure 8. The colored plane shows how the rotation speed can be tuned by adjusting the initial parameters (a) beam convergence angle and (b) aperture diameter both for DOEs and SLM.

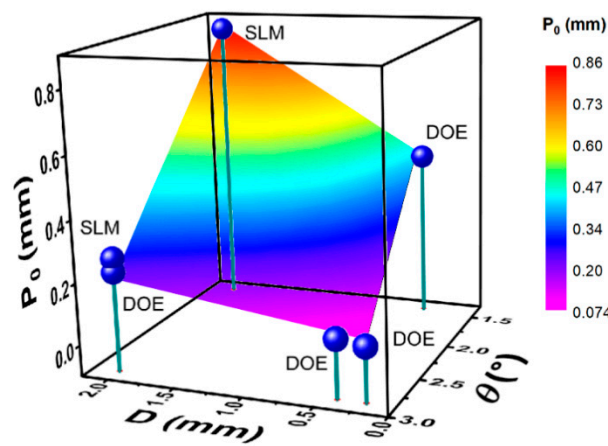


Figure 8. Axial rotation periods P_0 of the spectral eyes as a function of conical beam angle θ and element diameter D (DOE = fixed spiral grating, SLM = programmable spatial light modulator). It is indicated that both parameters can be used to control the spectral Gouy rotation.

The axial period of rotation grows with increasing diameter D and decreasing conical angle θ . The SPG periods of 16 μm and 32 μm correspond to conical half angles of the first diffraction orders of 2.87° and 1.43° , respectively. If the bandwidth is small enough, the components act like axicons and Gouy phase is continuously accumulated with increasing propagation distance. For the smallest elements, the diffraction at the aperture (outer rim of the element) influences the angular spectrum most. By calculating the “focal length” of a pinhole (Fresnel number ~ 1), one obtains a maximum angle of diffraction of $\theta_{max} \sim \arctan(\lambda/2D)$. For an element diameter of 200 μm and a wavelength of 800 nm, θ_{max} should be in the range of 0.115° .

In Figure 9, the continuously increasing rotation angle φ is plotted for extended propagation distances. The numbers correspond to the configurations in Table 1. The maximum number of rotations was about 10. The relative coordinate $z-z_j$ results from different starting points z_j of the zones of detectable rotation. The accumulated phase is found to be linear with small deviations, as is expected for Bessel-like beams. Linearity enables well-defined rotation control. For some curves, the ranges of parameters are not fully covered because some of the measurements had to be terminated for technical reasons like laser stability.

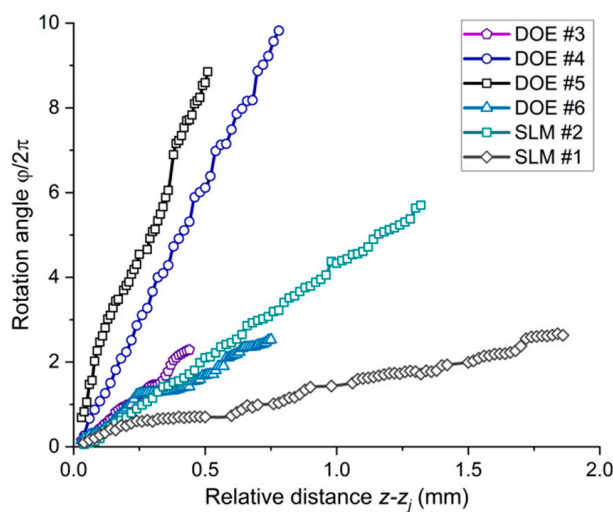


Figure 9. Angle of spectral Gouy rotation for extended propagation distances (numbers correspond to configuration numbers in Table 1). The increase of phase appears to be nearly linear.

To avoid misinterpretations, we would like to address the fact that the essential information in the curves is not a bandwidth transfer. The curves are plotted in pairs related to the spectral eyes; each upper curve of a pair corresponds to the red-shifted part, and each lower curve to the blue-shifted one. The ordinate values represent the spectral coordinates of the spectral eyes. The distance is not a measure of the output bandwidth, which is nearly constant because of conservation laws.

4.4. Rotation Control by Chirped Spirals and Multibeam Superposition

More sophisticated approaches for a control of the spectral Gouy rotation can be proposed on the basis of nonuniform phase shaping structures and by a coherent superposition [44]. In particular, an axially variable spectral rotation can be obtained by spiral gratings with radial gradients or spiral phase plates with appropriate phase profiles. By programming such structures in an SLM or steering the phase stroke of a radially curved spiral-phase MEMS mirror, the axial acceleration of rotation can even be tuned. Recently, it was shown that an angular frequency shift between two composite spiral phase zone plates can be used to adjust the wavefront rotation of an OAM beam [58].

The interference of two or more vortices of slightly different rotational velocities of their spectral eyes should also enable one to temporally modulate wavepackets. The “rotational beating” is expected to generate spectral “self-torque” analogous to a spin torque [43]. For two concentric, co-rotating wavepackets with angular velocities $\Omega_1(t)$ and $\Omega_2(t)$, we can define a spectral self-torque

$$\xi(t) = \frac{\partial[\Omega_2(t) - \Omega_1(t)]}{\partial t} \quad (8)$$

where the spectral eyes rotate with an angular frequency that periodically oscillates with the propagation distance (and, correspondingly, in time). The degree of rotational pulse stationarity depends on the ratio between pulse duration and beat frequency. If the oscillation is slow, the intrapulse spectral map can, approximately, be considered to be quasi stationary. If the oscillation is fast enough, however, an intrapulse rotational chirp should be detectable at each distance and time.

5. Conclusions

To conclude, a spectral Gouy rotation of ultrashort-pulsed and polychromatic OAM beams can be used as a further channel for information transfer and may find applications in metrology, optical processing, or selective excitation and manipulation. In particular, we have shown that the rotation of spectral eyes of propagating ultrashort vortex pulses can be controlled by governing the Gouy phase shift via selected angular and spectral parameters. The appearance of low-contrast spectral anomalies in the vicinity of singularities required one to work at relatively high spatial and spectral resolution and to develop adapted statistical tools for spectral image processing. Methods to generate axially accelerated spectral Gouy rotation were proposed. Currently, programmable radially chirped spiral phase gratings on the basis of liquid crystal spatial light modulators and MEMS are being studied. We introduced the concept of rotational “self-torque” in spectral domain. The effect should be obtainable by a superposition of multiple OAM pulses with different spectral Gouy rotation. The additional degrees of freedom enabled by axial rotational acceleration and spectral self-torque effects could find applications in singular optical processing.

Supplementary Materials: The following animations are available online at <http://www.mdpi.com/2076-3417/10/12/4288/s1>, video S1: Measured rotation of spectral eyes for a spiral grating programmed in an SLM (period 16 μm).

Author Contributions: Conceptualization, M.L., A.T., M.B., U.W., and R.G.; Data curation, M.L.; Methodology, M.L., A.T., and U.W.; Project administration, R.G.; Software, M.L., A.T., and M.B.; Supervision, R.G.; Visualization, M.L., A.T., and R.G.; Writing—original draft, M.L. and R.G.; Writing—review and editing, M.L., M.B., U.W., and R.G. All authors have read and agreed to the published version of the manuscript.

Funding: This research was funded by Deutsche Forschungsgemeinschaft, grant numbers GR1782/16-1 and WA1657/11-1.

Acknowledgments: We gratefully acknowledge design and fabrication of diffractive spiral gratings by J. Jahns, T. Seiler (FernUniversität Hagen) and Photonics MZD (Dresden). HOLOEYE Photonics (Berlin) provided advanced spatial light modulators. Light microscopy was performed in the laboratory of D. Engel (MBI).

Conflicts of Interest: The authors declare no conflict of interest.

References

1. Bazhenov, V.Y.; Soskin, M.S.; Vasnetsov, M.V. Screw dislocations in light wavefronts. *J. Mod. Opt.* **1992**, *39*, 985–990. [[CrossRef](#)]
2. Allen, L.; Barnett, S.M.; Padgett, M.J. *Optical Angular Momentum*; CRC Press: Bristol, UK, 2003.
3. Leach, J.; Keen, S.; Padgett, M.J.; Saunter, C.; Love, G.D. Direct measurement of the skew angle of the Poynting vector in a helically phased beam. *Opt. Express* **2006**, *14*, 11919–11924. [[CrossRef](#)] [[PubMed](#)]
4. Andrews, D.; Babiker, M. (Eds.) *The Angular Momentum of Light*; Cambridge University Press: Cambridge, UK, 2012.
5. Mann, A. ‘Twisted’ light beams promise an optical revolution. *PNAS* **2018**, *115*, 5621–5623. [[CrossRef](#)] [[PubMed](#)]
6. He, H.; Friese, M.E.J.; Heckenberg, N.R.; Rubinsztein-Dunlop, H. Direct observation of transfer of angular-momentum to absorptive particles from a laser-beam with a phase singularity. *Phys. Rev. Lett.* **1995**, *75*, 826–829. [[CrossRef](#)]
7. Garcés-Chávez, V.; Volke-Sepulveda, K.; Chávez-Cerda, S.; Sibbett, W.; Dholakia, K. Transfer of orbital angular momentum to an optically trapped low-index particle. *Phys. Rev. A* **2002**, *66*, 063402.
8. Shvedov, V.G.; Desyatnikov, A.S.; Rode, A.V.; Izdebskaya, Y.V.; Krolikowski, W.Z.; Kivshar, Y.S. Optical vortex beams for trapping and transport of particles in air. *Appl. Phys. A* **2010**, *100*, 327–331. [[CrossRef](#)]
9. Babiker, M.; Bennett, C.R.; Andrews, D.L.; Dávila Romero, L.C. Orbital angular momentum exchange in the interaction of twisted light with molecules. *Phys. Rev. Lett.* **2002**, *89*, 143601. [[CrossRef](#)]
10. Picón, A.; Mompart, J.; Vázquez de Aldana, J.R.; Plaja, L.; Calvo, G.F.; Roso, L. Photoionization with orbital angular momentum beams. *Opt. Express* **2010**, *18*, 3660–3671. [[CrossRef](#)]
11. Hnatovsky, C.; Shvedov, V.G.; Krolikowski, W.; Rode, A.V. Materials processing with a tightly focused femtosecond laser vortex pulse. *Opt. Lett.* **2010**, *35*, 3417–3419. [[CrossRef](#)]
12. Hamazaki, J.; Morita, R.; Chujo, K.; Kobayashi, Y.; Tanda, S.; Omatsu, T. Optical-vortex laser ablation. *Opt. Express* **2010**, *18*, 2144–2151. [[CrossRef](#)]
13. Ni, J.; Wang, C.; Zhang, C.; Hu, Y.; Yang, L.; Lao, Z.; Xu, B.; Li, J.; Wu, D.; Chu, J. Three-dimensional chiral microstructures fabricated by structured optical vortices in isotropic material. *Light Sci. Appl.* **2017**, *6*, e17011. [[CrossRef](#)] [[PubMed](#)]
14. Omatsu, T.; Miyamoto, K.; Toyoda, K.; Morita, R.; Arita, Y.; Dholakia, K. A New Twist for Materials Science: The formation of chiral structures using the angular momentum of light. *Adv. Opt. Mat.* **2019**, *7*, 1801672. [[CrossRef](#)]
15. Tamburini, F.; Anzolin, G.; Umbriaco, G.; Bianchini, A.; Barbieri, C. Overcoming the Rayleigh criterion limit with optical vortices. *Phys. Rev. Lett.* **2006**, *97*, 163903. [[CrossRef](#)]
16. Crabtree, K.; Davis, J.A.; Moreno, I. Optical processing with vortex-producing lenses. *Appl. Opt.* **2004**, *43*, 11360–11367. [[CrossRef](#)]
17. Gibson, G.; Courtial, J.; Padgett, M.J.; Vasnetsov, M.; Pas’ko, V.; Barnett, S.M.; Franke-Arnold, S. Free-space information transfer using light beams carrying orbital angular momentum. *Opt. Express* **2004**, *12*, 5448–5456. [[CrossRef](#)] [[PubMed](#)]
18. Lavery, M.P.J.; Tur, M.; Ramachandran, S.; Molisch, A.F.; Ashrafi, N.; Ashrafi, S. Optical communications using orbital angular momentum beams. *Adv. Opt. Phot.* **2015**, *7*, 66–106.
19. Cozzolino, D.; Bacco, D.; Da Lio, B.; Ingerslev, K.; Ding, Y.; Dalgaard, K.; Kristensen, P.; Galili, M.; Rottwitt, K.; Ramachandran, S.; et al. Orbital angular momentum states enabling fiber-based high-dimensional quantum communication. *Phys. Rev. Appl.* **2019**, *11*, 064058. [[CrossRef](#)]
20. Wang, J.; Yang, J.Y.; Fazal, I.M.; Ahmed, N.; Yan, Y.; Huang, H.; Ren, Y.; Yue, Y.; Dolinar, S.; Tur, M.; et al. Terabit free-space data transmission employing orbital angular momentum multiplexing. *Nat. Photon.* **2012**, *6*, 488–496. [[CrossRef](#)]

21. Wang, X.; Nie, Z.; Liang, Y.; Wang, J.; Li, T.; Jia, B. Recent advances on optical vortex generation. *Nanophotonics* **2018**, *7*, 1533–1556. [[CrossRef](#)]
22. Shen, Y.; Wang, X.; Xie, Z.; Min, C.; Fu, X.; Liu, Q.; Gong, M.; Yuan, X. Optical vortices 30 years on: OAM manipulation, from topological charge to multiple singularities. *Light Sci. Appl.* **2019**, *8*, 90. [[CrossRef](#)]
23. Dorrah, A.H.; Rosales-Guzmán, C.; Forbes, A.; Mojahedi, M. Evolution of orbital angular momentum in three-dimensional structured light. *Phys. Rev. A* **2018**, *98*, 043846. [[CrossRef](#)]
24. Yang, Y.; Zhu, X.; Zeng, J.; Lu, X.; Zhao, C.; Cai, Y. Anomalous Bessel vortex beam: Modulating orbital angular momentum with propagation. *Nanophotonics* **2018**, *7*, 677–682. [[CrossRef](#)]
25. Rozas, D.; Law, C.T.; Swartzlander, G.A. Propagation dynamics of optical vortices. *J. Opt. Soc. Am. B* **1997**, *14*, 3054–3065. [[CrossRef](#)]
26. Porras, M.A. Upper bound to the orbital angular momentum carried by an ultrashort pulse. *Phys. Rev. Lett.* **2019**, *122*, 123904. [[CrossRef](#)] [[PubMed](#)]
27. Gbur, G.; Visser, T.D.; Wolf, E. Anomalous behavior of spectra near phase singularities of focused waves. *Phys. Rev. Lett.* **2002**, *88*, 01390. [[CrossRef](#)]
28. Berry, M.V. Coloured phase singularities. *New J. Phys.* **2002**, *4*, 66–73. [[CrossRef](#)]
29. Berry, M.V. Exploring the colours of dark light. *New J. Phys.* **2002**, *4*, 74–80. [[CrossRef](#)]
30. Popescu, G.; Dogariu, A. Spectral anomalies at wave-front dislocations. *Phys. Rev. Lett.* **2002**, *88*, 183902. [[CrossRef](#)]
31. Leach, J.; Padgett, M.J. Observation of chromatic effects near a white-light vortex. *New J. Phys.* **2003**, *5*, 154. [[CrossRef](#)]
32. Angelsky, O.V.; Hanson, S.G.; Maksimyak, A.P.; Maksimyak, P.P. Feasibilities of interferometric and chromoscopic techniques in study of phase singularities. *Appl. Opt.* **2005**, *44*, 5091–5100. [[CrossRef](#)]
33. Zapata-Rodríguez, C.J. Analytical characterization of spectral anomalies in polychromatic aperture beams. *Opt. Commun.* **2006**, *257*, 9–15. [[CrossRef](#)]
34. Ding, C.; Pan, L.; Lü, B. Phase singularities and spectral changes of spectrally partially coherent higher-order Bessel-Gauss pulsed beams. *J. Opt. Soc. Am. A* **2009**, *26*, 2654–2661. [[CrossRef](#)] [[PubMed](#)]
35. Bock, M.; Grunwald, R. Mapping the spectral twist of few cycle vortex pulses. *Proc. SPIE* **2016**, 9764, 97640O.
36. Bock, M.; Liebmann, M.; Elsaesser, T.; Grunwald, R. *Gouy Phase Rotation in Spectral Maps of Ultrashort Vortex Pulses*; Digest Paper EE-1.4; CLEO/Europe-EQEC: Munich, Germany, 2017.
37. Liebmann, M.; Treffer, A.; Bock, M.; Elsaesser, T.; Grunwald, R. Spectral anomalies and Gouy rotation around the singularity of ultrashort vortex pulses. *Opt. Express* **2017**, *25*, 26076–26088. [[CrossRef](#)]
38. Baumann, S.M.; Kalb, D.M.; MacMillan, L.H.; Galvez, E.J. Propagation dynamics of optical vortices due to Gouy phase. *Opt. Express* **2009**, *17*, 9818–9827. [[CrossRef](#)] [[PubMed](#)]
39. Hamazaki, J.; Mineta, Y.; Oka, K.; Morita, R. Direct observation of Gouy phase shift in a propagating optical vortex. *Opt. Express* **2006**, *14*, 8382–8392. [[CrossRef](#)]
40. Miyahara, H.; Qi, Y.; Kurihara, T.; Ando, S. Rotation of multi-zeros optical beam during propagation and its application to distance measurement. In Proceedings of the SICE Annual Conference 2011, Tokyo, Japan, 13–18 September 2011. FrC03-06.
41. Schulze, C.; Roux, F.S.; Dudley, A.; Rop, R.; Duparré, M.; Forbes, A. Accelerated rotation with orbital angular momentum modes. *Phys. Rev. A* **2015**, *91*, 043821. [[CrossRef](#)]
42. Yamane, K.; Sakamoto, M.; Murakami, N.; Morita, R.; Oka, K. Picosecond rotation of a ring-shaped optical lattice by using a chirped vortex-pulse pair. *Opt. Lett.* **2016**, *41*, 4597–4600. [[CrossRef](#)]
43. Rego, L.; Dorney, K.M.; Brooks, N.J.; Nguyen, Q.L.; Liao, C.-T.; Román, J.S.; Couch, D.E.; Liu, A.; Pisanty, E.; Lewenstein, M.; et al. Generation of extreme-ultraviolet beams with time-varying orbital angular momentum. *Science* **2019**, *364*, eaaw9486. [[CrossRef](#)]
44. Liebmann, M.; Treffer, A.; Bock, M.; Wallrabe, U.; Grunwald, R. Controlling the spectral rotation of ultrashort vortex pulses. *Proc. SPIE* **2020**, 11297, 112970W.
45. Gouy, L.G. Sur une propriété nouvelle des ondes lumineuses. *C. R. Acad. Sci. Paris* **1890**, *110*, 1251–1253.
46. Gouy, L.G. Sur la propagation anormale des ondes. *Compt. Rendue Acad. Sci. Paris* **1890**, *111*, 33–35.
47. Rubinowicz, A. On the anomalous propagation of phase in the focus. *Phys. Rev.* **1938**, *54*, 931–936. [[CrossRef](#)]
48. Boyd, R.W. Intuitive explanation of the phase anomaly of focused light beams. *J. Opt. Soc. Am.* **1980**, *70*, 877–880. [[CrossRef](#)]

49. Kim, M.-S.; Scharf, T.; da Costa Assafrao, A.; Rockstuhl, C.; Pereira, S.F.; Urbach, H.P.; Herzig, H.P. Phase anomalies in Bessel-Gauss beams. *Opt. Express* **2012**, *20*, 28929–28940. [[CrossRef](#)] [[PubMed](#)]
50. Martelli, P.; Tacca, M.; Gatto, A.; Moneta, G.; Martinelli, M. Gouy phase shift in nondiffracting Bessel beams. *Opt. Express* **2010**, *18*, 7108–7120. [[CrossRef](#)]
51. Liebmann, M.; Treffer, A.; Bock, M.; Seiler, T.; Jahns, J.; Elsaesser, T.; Grunwald, R. Spectral self-imaging and Gouy rotation echoes of propagating vortex pulse arrays. *Proc. SPIE* **2019**, *10935*, 109350T.
52. Liebmann, M.; Treffer, A.; Bock, M.; Seiler, T.; Jahns, J.; Elsaesser, T.; Grunwald, R. Self-imaging of tailored vortex pulse arrays and spectral Gouy rotation echoes. *Opt. Lett.* **2019**, *44*, 1047–1050. [[CrossRef](#)]
53. Musigmann, M.; Jahns, J.; Bock, M.; Grunwald, R. Refractive-diffractive dispersion compensation for optical vortex beams with ultrashort pulse durations. *Appl. Opt.* **2014**, *53*, 7304–7311. [[CrossRef](#)]
54. Bock, M.; Brunne, J.; Treffer, A.; König, S.; Wallrabe, U.; Grunwald, R. Sub-3-cycle vortex pulses of tunable topological charge. *Opt. Lett.* **2013**, *38*, 3642–3645. [[CrossRef](#)]
55. Liebmann, M.; Treffer, A.; Bock, M.; Seiler, T.; Jahns, J.; Elsaesser, T.; Grunwald, R. Spectral meta- moments reveal hidden signatures of vortex pulses. In Proceedings of the EPJ Web of Conferences, Beijing, China, 19–24 May 2019; Volume 205, p. 01005.
56. Yadav, B.K.; Kandpal, H.C. Spectral anomalies of polychromatic DHGB and its applications in FSOJ. *Lightwave Technol.* **2011**, *29*, 960–966. [[CrossRef](#)]
57. Pu, J.; Cai, C.; Nemoto, S. Spectral anomalies in Young’s double-slit interference experiment. *Opt. Express* **2004**, *12*, 5131–5139. [[CrossRef](#)] [[PubMed](#)]
58. Ghebjagh, S.G.; Sinzinger, S. Composite spiral multi-value zone plates. *Appl. Opt.* **2020**, *15*, 4618–4623. [[CrossRef](#)] [[PubMed](#)]



© 2020 by the authors. Licensee MDPI, Basel, Switzerland. This article is an open access article distributed under the terms and conditions of the Creative Commons Attribution (CC BY) license (<http://creativecommons.org/licenses/by/4.0/>).